DOE/BC/15207-2

(OSTI ID: 807246)

Experimental Investigation of Relative Permeability Upscaling from the Micro-Scale to the Macro-Scale

Semi-Annual Progress Report

Reporting Period Start Date: September 1, 2000
Reporting Period End Date: Feb 28, 2000

Ping Yu, Nicholas Giordao, JiangTao Cheng, Mirela Mustata , William Headley, Daiquan Chen, Nathan Cooper, David D. Nolte and Laura J. Pyrak-Nolte

March 2001

DOE Award: DE-AC26-99BC15207

Purdue Research Foundation
Department of Physics
1396 Physics Building, Room 166
West Lafayette, Indiana 47907-1396

Abstract: The principal challenge of upscaling techniques for multi-phase fluid dynamics in porous media is to determine which properties on the micro-scale can be used to predict macroscopic flow and spatial distribution of phases at core- and field-scales. The most notable outcome of recent theories is the identification of interfacial areas per volume for multiple phases as a fundamental parameter that determines much of the multi-phase properties of the porous medium. A formal program of experimental research was begun to directly test upscaling theories in fluid flow through porous media by comparing measurements of relative permeability and capillary-saturation with measurements of interfacial area per volume. During this reporting period, we achieved the milestone of using Optical Coherence Imaging (OCI) to image to the back of the first layer of grains in a sandstone sample. This is the first time that OCI has been used to image through sandstone. Information on grain geometry was obtained as deep as 400 microns into the sample. This report also describes the work performed to achieve the milestone on the measurement of interfacial area per volume, capillary pressure and saturation in two dimensional micro-models structures that are statistically similar to real porous media. This report contains the first quantitative experimental measurements of interfacial area per volume in any system.

Table of Contents

List of Figures

List of Tables

Executive Summary

Direct experimental tests of upscaling theories in fluid flow through porous media will be made by comparing measurements of relative permeability and capillary-saturation with measurements of interfacial area per volume. These experiments are performed from the pore-scale (microns) to the core-scale (centimeters), spanning four orders of magnitude in size. Three experimental objectives provide the data for rigorous tests of upscaling theories. First, holographic laser imaging techniques will acquire pore-scale three-dimensional optical images of the pore geometry in reservoir sandstones. This technique uses unique properties of coherent light to see through drilling muds and into the sandstone. Second, laboratory micro-models with matched topological properties based on the data from the pore imaging will make it possible to measure interfacial area per volume in scientifically controlled imbibition and drainage experiments, combined with measurements of capillary-pressure-saturation data and relative permeability. Third, core-scale experiments of relative permeability and capillary-saturation, and metal casts of the pore geometry, will be compared with the pore-scale data of the first two objectives. The data from all these objectives will provide the first complete picture over such a large dynamic range. It will make it possible to answer the principal question concerning flow upscaling: which microscopic measurements are most useful for predicting macroscopic flow properties of an oil reservoir. The tangible outcome of this work will be explicit data connecting interfacial areas, or other relevant geometric micro-scale data, with macroscopic hydraulic properties. In addition, we show strong industrial interest in testing and commercializing the unique down-hole laser imaging technology that can be transferred to the oil-industry service-company sector.

We achieved the milestone for this reporting period of using Optical Coherence Imaging (OCI) to image to the back of the first layer of grains in a sandstone sample. This is the first time that OCI has been used to image through sandstone. Information on grain geometry was obtained as deep as 400 microns into the sample.

This report also describes the work performed to achieve the milestone on the measurement of interfacial area per volume, capillary pressure and saturation in two dimensional micro-models structures that are statistically similar to real porous media. This report contains the first quantitative experimental measurements of interfacial area per volume in any system.

1.0 Introduction

1.1 BACKGROUND

1.1.1 Summary of Project Description

Standard expressions of multi-phase flow in porous media based on modifications of Darcy's Law (Darcy, 1856) have crippling deficiencies that make them undesirable to use for critical operations such as tertiary recovery of oil from depleted reservoirs. The primary difficulty in these empirical expressions are their violation of rigorous conservation laws. New theories based on rigorous volume averaging theorems and fundamental thermodynamic principles of phase boundaries have emerged in the past decade to replace the old empirical rules (Hassanizadeh and Gray, 1979; Gray, 1983; Kalaydjian, 1990). The most notable outcome of these theories is the identification of interfacial areas per volume for multiple phases as fundamental parameters that determine much of the multi-phase properties of the porous medium (Muccino, Gray and Ferrand, 1998).

Interfacial areas per volume provide natural descriptions of fundamental physical processes in porous media. For instance, thermodynamic energies are proportional to interfacial areas, and interfacial areas per volume represent a form of energy density. Gradients in energy densities define the dynamical pressures that drive the movement and distribution of phases within a complex topology. Interfacial areas per volume in a porous medium therefore represent a three-dimensional potential energy landscape.

Interfacial areas per volume also provide a natural yard-stick for defining the role of scale in multiphase fluid properties. The dimensional units of interfacial area per volume is a spatial frequency (inverse length) that breaks scale invariance. A useful illustration (Gray, 1998) of this scale-defining role can be made by considering an image of a pore-geometry containing only a single phase. Without a measurement scale, it is impossible to state what the physical size of the system is. However, when two phases such as water and air are both

present, the length scale becomes obvious. At small scales, the water-air interface is drawn into the pore throats, while at large scales the water puddles in the large void volumes.

Therefore, the interfacial areas between phases define a length scale. Whenever a physical system has an intrinsic length scale, the physics of the system can be divided into two regimes: one where sample sizes are larger than the intrinsic length scale, and the other where information is obtained on scales smaller than the intrinsic length scale. Breaking scale invariance makes it possible to define representative elementary volumes (REV) and to apply averaging theorems. Combining the averaging theorems with thermodynamics further constrains the possible types of constitutive equations that can rigorously describe multiphase fluid properties in porous media.

As a consequence of this theoretical framework, interfacial areas per volume (IAV) take on a more important role than simple volume saturation . This important role of IAV is clear because a single value of relative volume saturation can correspond to infinitely different distributions of two phases within the volume. Large values of IAV relate to a finely distributed phase that can block pore throats and seriously affect permeability, while small values of IAV relate to gross separations of phases, with large connected volumes of the phase that can flow unimpeded through the network. Significant numerical studies have been performed on the relationships between capillary-saturation and interfacial area. Reeves and Celia (1995) developed a numerical model that scans over repetitive imbibition and drainage while tracking the interfacial area for each loop. These studies pointed to a non-unique relationship between interfacial area and partial saturation, although a family of curves did emerge that lies within a localized part of the parameter space defined by area and saturation.

The numerical studies illustrate the importance of continued and extensive experimental studies and tests of upscaling theories, and in particular tests of the role of interfacial area per volume in determining macroscopic flow properties. While oil recovery predictions should certainly include IAV as critical parameters, it is important to test whether other microscopic parameters also contribute to the macroscopic behavior. For instance, scale invariance of

interfacial areas, even over restricted length scales, could present serious challenges to the averaging theorems, and could modify the presumed role of interfacial area in determining macroscopic flow properties. The principal objective of our proposed upscaling approach is to experimentally measure many microscopic geometric parameters of the flow system over many scales, and connect these microscopic measurements with macroscopic flow behavior.

1.1.2 OCI Milestone Background

The principal challenge of upscaling techniques for multi-phase fluid dynamics in porous media is to determine which properties on the micro-scale can be used to predict macroscopic flow and spatial distribution of phases at core- and field-scales. First-principles theoretical formulations over the past decade have been derived from rigorous volume averaging theorems in which microscopic interfacial behavior is explicitly incorporated. In contrast to the traditional importance placed on volume saturation, these theories have proposed that interfacial areas per volume more directly predict macroscopic behavior, and that this variable may govern the observed hysteresis in saturation-capillary pressure relationships.

Despite the importance of testing interfacial theories, interfacial areas per volume are considerably more difficult to measure than the traditional partial volume saturations. Volumes can be measured by simple volume displacements, by weight, or by attenuation coefficients in commercial radiation logging apparatus. Interfacial areas inside opaque rock, on the other hand, have been largely inaccessible. Most advanced imaging techniques do not have the appropriate spatial resolution to measure interfacial areas at the pore-scale. Although several imaging techniques have made inroads to this problem, such as x-ray microtomography, confocal microscopy and metal-injection, these techniques have not previously provided information appropriate for the testing of upscaling theories.

For the work for this project, an advanced optical imaging technique is being developed to acquire volumetric pore geometry of representative reservoir sandstone cores at the micron-scale. The imaging data will be used to reconstruct the pore geometry in the laboratory using fabrication techniques from the semiconductor micro-circuit industry (Giordano and Cheng, 2001). These synthetic micromodels are highly controlled, have feature sizes down to microns, extend over millimeters, and will allow us obtain accurate

measurements of relative permeability, capillary-pressure-saturation, as well as the important interfacial areas per volume. The tangible outcome of these experiments are explicit experimental curves capillary-saturation to the interfacial areas per volume of two fluid phases and one solid phase.

This report describes the work performed for the milestone on the use of the Optical Coherence Imaging (OCI) to image to the back of the first layer of grains in a rock core. Optical Coherence Imaging is an advancement on Optical Coherence Tomography (OCT) which is a well-established laser imaging technique for imaging through translucent media (Izatt, Kulkarni, et al., May, 1997). OCT has been most commonly applied to shallow imaging through biological tissue (Izatt, Kulkarni, et al., 1996; Pan, Lankenau, et al., 1996; Tearney, Brazinski, et al., 1997) . The principal of operation for OCT relies on the coherent nature of laser light. When laser light propagates through a translucent medium, part of the light scatters off optical heterogeneities, while part continues to propagate unscattered, and reflects off buried objects of interest. This unscattered light is sometimes called "ballistic" light (Wang, Ho, et al., 1991) .

The difficulty of imaging through scattering media is that the scattered light obscures the image of interest carried by the ballistic light. However, the scattered and unscattered light have one very different property -- the unscattered light remains coherent with the original laser beam. The basic process of OCT is to detect only the coherent light, rejecting the incoherent scattered light.

This "coherence detection" has been used successfully in conventional OCT systems that use a simple interferometer. By changing the length of one of the arms in the interferometer, the light is collected from different depths in the specimen and OCT gives full three-dimensional data. It performs like a laser ranging system, except that the laser light can penetrate into a translucent object.

While conventional OCT is a promising optical technology for imaging into systems that were previously inaccessible, it performs point-by-point scanning, which is time consuming, and is not compatible with imaging directly to a video televiewer screen for the operator to see.

Optical Coherence Imaging is based on the same principals as OCT but acquires full-frame images. OCI uses the coherence of the ballistic light -- and the incoherence of the

unwanted obscuring light -- to make an optical hologram of only the light carrying the image of interest [Jones, Hyde, et al., 1996] . Because the coherence detector is a hologram, it captures a full image in a single shot [Hyde, Jones, et al., 1996]. Therefore, this penetrating-imaging system can acquire actual video images that can be viewed in real time on a televiewer, and recorded on a video cassette [Jones, et al., 1998]. This has an advantage over other penetrating-imaging processes, such as confocal microscopy, which must scan point-by-point.

These previous OCI demonstrations have been primarily used for free-space three-dimensional topography and for imaging through turbid media. No previous work has attempted to image into materials such as sandstone because it was previously thought that the static structure of the sandstone would produce strong laser speckle that would obscure the hologram. In the experiments reported here we have used a vibrating mirror to cause the laser speckle from the sandstone to time-average on the video camera. This removes the speckle problem for the imaging, and the work contained in this report represents the first use of OCI to image into rock. We have been able to see as deep as 400 microns into the rock, and have delineated the geometric shapes of several sand grains from stacks of holographic images. We therefore have achieved the contracted milestone and are well on our way towards further goals of this research project.

1.1.3 Micro-Model Milestone Background

Fluid flow in porous media is generally described using Darcy's law (Darcy, 1856). This "law" was originally developed to describe single phase flow. It provides a good and much used description of single phase flow. However, many cases of interest involve two or more fluid phases that are flowing (or at least present) simultaneously; i.e., multi-phase flow. There have been many efforts to extend Darcy's law to this problem, but all involve serious approximations or assumptions. While such extensions of Darcy's law are widely used, it is also well known that they fail in some important regimes (Muccino, Gray, and Ferrand, 1998), and that a better theoretical description is urgently needed. One alternative to Darcy's law has been developed over the past decade or so (Hassanizadeh and Gray, 1979; Gray, 1983; Kalaydjian, 1990; Muccino, Gray, and Ferrand, 1998). This work predicts that the interfacial area per unit volume is a fundamental variable that must be included along with

the more traditional variables such as capillary pressure and saturation, in order to provide an accurate and fundamentally sound description of fluid flow. One of the primary objectives of this project is to test this theoretical prediction.

The traditional description of multiphase flow employs variables such as capillary pressure (P_{cap}), saturation (S) and relative permeability. These quantities can be measured in real or artificial porous materials, so theories which involve only these quantities, such as Darcy's law, can be readily compared with experiment. However the theoretical work referenced above predicts that other variables are also essential for the understanding, description, and prediction of flow behavior in a multi-phase system. The measurement of the interfacial area per unit volume (*IAV*) for two fluid phases in contact is quite challenging for a number of reasons, especially in opaque materials such as rock. While it is difficult to measure *IAV* in real materials, it is possible to design artificial porous materials, so-called micro-models, in which the *IAV* can be measured quantitatively. There are several types of micro-models (Giordano and Cheng, 2001), but all are functionally similar to the ones studied in this project. As will be described in detail in Section 2, our micro-models are two dimensional structures in which a flow geometry is formed in a thin polymer layer deposited onto a glass plate. The top of the polymer layer is sealed with a second glass plate, forming a pattern of open area in which one or more fluid phases can move.

Such micro-models have been studied for a number of years (Wardlaw, 1982; Lenormand, Zarcone, and Starr, 1983; Lenormand and Zarcone, 1989; Soll, Cella, and Wilson, 1993; Giordano and Cheng, 2001). They have been used to study flow properties (i.e., relative permeability), and also to learn about the spatial geometry of the phases in multi-phase flow. However, to the best of our knowledge, the measurement of flow and geometry have always been made separately, and there is no available data on both as measured simultaneously on a given sample. In addition, the measurements of spatial geometry have only given information about individual phases. For example, the fractal pattern of a single invading fluid phase has been measured (Lenormand and Zarcone, 1989), but there have not yet been any measurements of the relative arrangement of multiple phases; i.e., there have been no measurements of *IAV*. The experimental results presented in Section 2 are the first measurements of this quantity in any system.

One of the goals of this project is to study multiphase flow in micro-models, and to perform quantitative measurements of $P_{cap,}S$, and *IAV* so as to test the theories mentioned above. In order to relate the relatively idealized micro-model systems to more realistic materials, we have constructed special micro-models with geometries designed to match those measured in the Wood's metal task of this project, where data on real sandstone have been obtained.

1.2 OBJECTIVES

1.2.1 PROJECT OBJECTIVES

The proposed work for this contract has three objectives that will provide rigorous experimental tests of upscaling theories. The objectives are:

1) To use holographic laser imaging techniques to acquire pore-scale three-dimensional optical images of the pore geometry in reservoir sandstones. This technique uses unique properties of coherent light to see through drilling muds and up to a millimeter into the sandstone. This data forms the basis of upscaling experiments to test theories of interfacial area per volume.

2) To construct laboratory micro-models with matched topological properties based on the data from the pore imaging. Interfacial area per volume will be measured directly in controlled imbibition and drainage experiments, together with capillary-pressure-saturation data and relative permeability data. This set of interrelated data will allow rigorous testing of upscaling theories.

3) To perform core-scale experiments of relative permeability and capillary-saturation, and to make metal casts of the pore geometry and interfacial area per volume. This core-scale data (including pore-scale from the metal casts) will be compared with the pore-scale data of the first two objectives, extending the observation scales over four orders of magnitude.

1.2.2 OCI Milestone Objective

One of the objectives for the work for this contract involves the use of a holographic laser imaging technique (Optical Coherence Imaging) to acquire pore-scale three-dimensional optical images of the pore geometry in reservoir-like sandstones. This technique uses unique properties of coherent light to see through drilling muds and up to a millimeter into the sandstone. This data forms the basis of upscaling experiments to test theories of interfacial area per volume.

The objective for this milestone report is to use Optical Coherence Imaging (OCI) to image to the back of the first layer of grains in a rock core.

1.2.3 Micro-Model Milestone Objective

The objective for the micro-model task during this reporting period is to study and obtain quantitative results for multiphase flow in micro-models, through measurements of the interfacial area, capillary pressure, saturation, and absolute and relative permeability. This goal has been achieved through the following work.

- We have designed and installed improved lithographic facilities required for micro-model fabrication.
- An improved apparatus for single and multiphase flow measurements has been designed and constructed.
- The above equipment has been tested, and we have developed analysis methods for the accurate measurement of *IAV* in micro-models.
- We have performed initial measurements of $P_{cap,}$ S, and *IAV* and permeability on micro-models with idealized geometries and with geometries designed to match (in a statistical sense) those obtained from the Wood's metal injection measurements.

2.0 Results and Discussion

2.1 Optical Coherence Imaging

2.1.1 Experimental Set-Up

An Optical Coherence Imaging (OCI) system was developed for this project to investigate the use of optical coherence imaging for imaging into the sandstone. The OCI system (Figure 1) consists of a mode-locked Ti:sapphire laser (120 femtoseconds (fs) pulses with 100 MHz repetition rate), a modified Mach Zehnder interferometer with a sample arm and a reference arm, and a photorefractive multiple quantum well (PRQW) device[Nolte, D.D., 1999] that is the dynamic holographic film. An electric field (DC 10 kV/cm) is applied in the plane of the device. This configuration is called transverse-field geometry that uses the

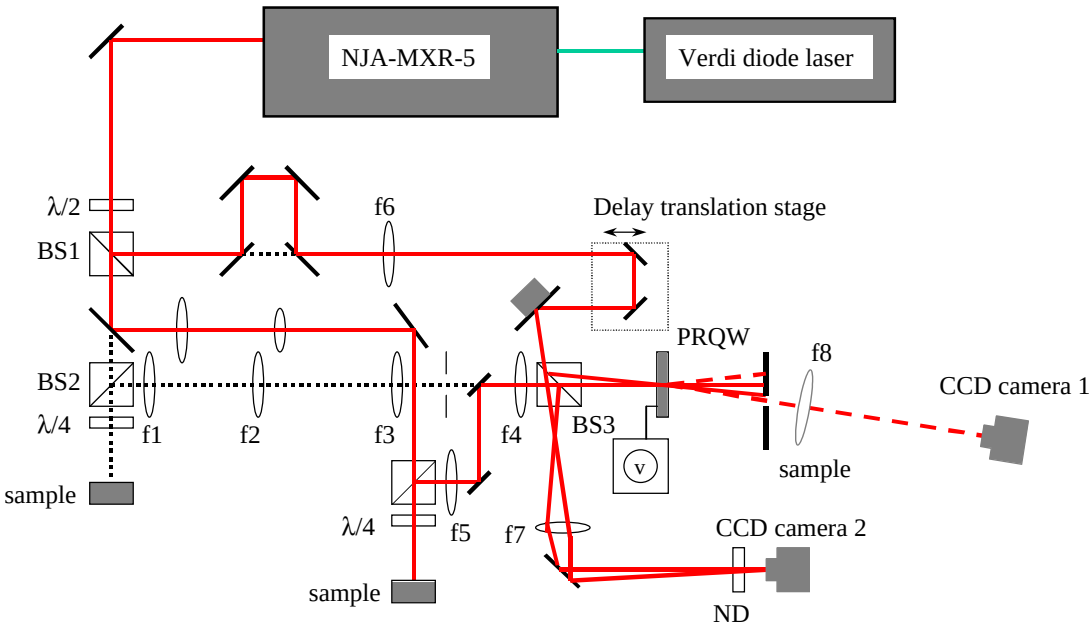

BS1, BS2: polarization beam splitter. BS3: 50/50 beam splitter.
f1=200mm, f2=100mm, f3=150mm, f4=f5=150mm, f6=500mm, f7=50mm, f8=150mm.
ND: Neutral Density Filter

Figure 1. The design and modifications of optical coherence imaging. The red lines represent the modified setup and the dash lines are from original setup.

Franz-Keldysh effect. In the interferometer, a de-magnified telescope (4:1) is used in the detecting arm that decreases the beam diameter to 1.0 mm on the sample. As a result, the intensity increases about 16 times at the sample. Two lenses with the same 150 mm focal length are separated by twice the focal length to form a 4-F system (Figure 2).

In this 4-F system, the sample is placed at the focal plane in front of the first lens and the PRQW device is placed at the focal plane in back of the second lens (Figure 2). The plane that is halfway between the lenses is called the Fourier plane or the transform plane. The 4-F system projects a 1:1 image of the sample onto the holographic film. A spatial filter is located at the Fourier plane of the 4-F system to reject part of the scattered light from the sample, and allow the ballistic components to travel to the device. The signal beam is interfered with the reference beam when the optical path lengths between the signal and reference arms are matched to within a coherence length of the laser by adjusting the translation stage in the reference arm. The interference fringes are imprinted onto the holographic film. The holograms are reconstructed using a degenerate four-wave mixing configuration. The first order

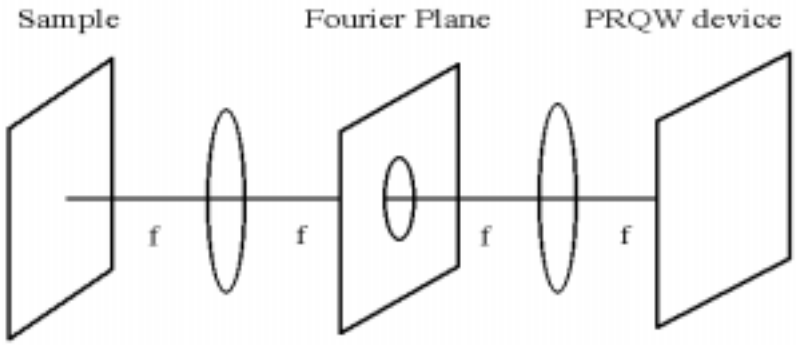

Figure 2. Two lenses form a 4-F configuration to get 1:1 imaging between the sample and PRQW device.

diffracted signal from the reference beam is imaged onto the surface of a cooled CCD camera (RTE/CCD 1317, Princeton Instruments) with a 150 mm focal length lens, while an aperture is used to cut off zero order beam. The efficiency of the four-wave mixing is optimized by

adjusting the wavelength and bandwidth of the laser, the size and position of the aperture, and the relative intensities between the signal and reference beams.

2.1.2 System Calibration

To test the resolution of the OCI system, a United States Air Force (USAF) test chart is used as the control image because it has calibrated bars of varying sizes. The layout of the USAF test chart is shown in Figure 3 and the sizes of the bars are listed in Table 1. Figure 4 (a) is a direct image recorded by the CCD camera 2 in Figure 1 using the fs-laser (center wavelength of 838 nanometer (nm) and bandwidth of 12 nm). The hologram of the test chart in figure 4b shows that the bar of element 5 at group 5 can be resolved, which means the lateral resolution of the OCI system is 10 μm. In figure 4 (b), the size of the hologram is 1.0 mm in diameter and is limited by the finite size of the beam.

The depth resolution of the OCI system was also calibrated using the United States Air Force (USAF) test chart. The reference pulse determines the depth in the sample at which the hologram is recorded. The arrival time of the reference pulse is controlled by a delay stage, i.e., a mirror mounted on a translation stage. The depth resolution is set by the coherence length of the laser (30 microns for the laser used in this experiment).

Figure 5 (a) shows the brightest hologram of the USAF test chart in the y-z plane. In figure 5 and the following figures, we define the coordinate system with the x axis along direction of light propagation. The hologram image plane is in y-z plane and the cross section that shows the depth information is in x-z or x-y plane. The size of the hologram recorded in the CCD camera represents the area of 500 μm ×700 μm on the holographic film, and is the same area on the sample, i.e., 1:1 imaging. The bars in the group 4 of the USAF test chart (Figure 3) are clearly observed where the bar labeled number one has a line width of 31 μm. Figure 5 (b) shown the depth-resolved holograms shown in cross sections (x-y plane and x-z plane). The three dark spots in the bright line at the upper half part in x-z plane are from the bars of the USAF test chart. The bright lines consist of 3 holograms at successive depths in the x direction for 10 μm increment between the images. The value of 30 μm is roughly equal to the depth resolution calculated from the coherence length of the fs-laser used in this experiment.

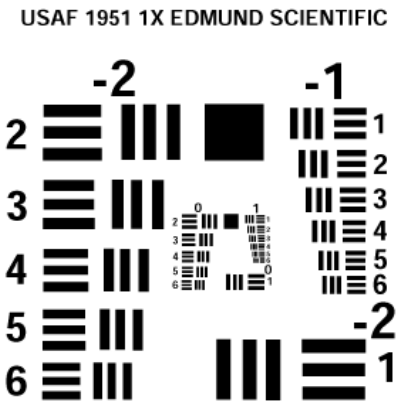

Figure 3. USAF test chart labeled with the sizes of the bars.

Table 1. The line width (in μm) of the bars of USAF test chart in different groups and element numbers.

	Group No.							
Element No.	**0**	**1**	**2**	**3**	**4**	**5**	**6**	**7**
1	500	250	125	62.5	31.25	15.63	7.81	3.91
2	446.43	223.21	111.36	55.68	27.86	13.89	6.96	3.47
3	396.83	198.41	99.21	49.50	24.80	12.41	6.20	3.11
4	354.61	176.68	88.34	44.25	22.10	11.04	5.52	2.76
5	314.47	157.73	78.74	39.37	19.69	9.84	4.90	2.46
6	280.90	140.45	70.13	34.97	17.54	8.77	4.39	2.19

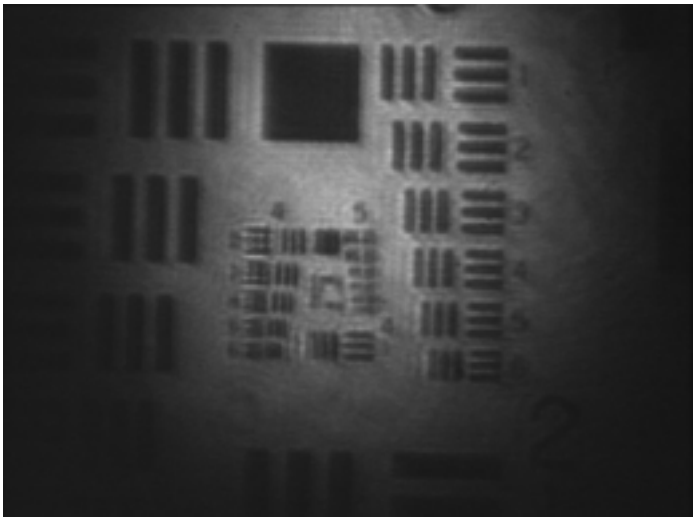

(a)

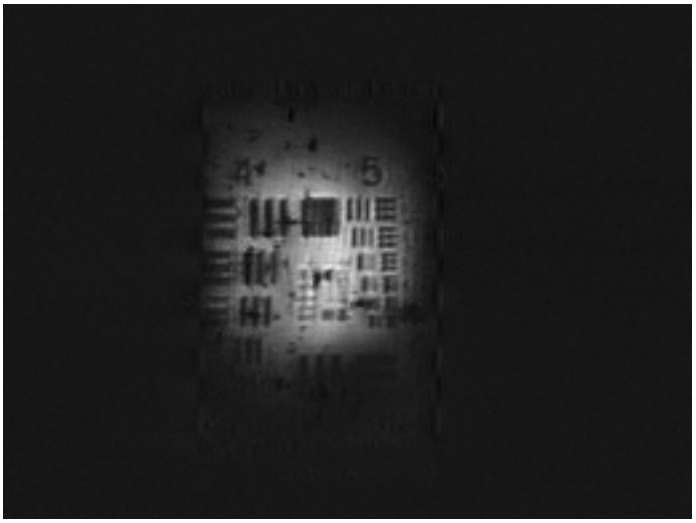

(b)

Figure 4. Direct image (a) and hologram (b) of USAF test chart. In the hologram, the minimum bar that can be resolved is element 5 at group 5. The full area of the picture represents 3x2 mm^2 on the sample plane.*(See electronic version for higher image quality)*

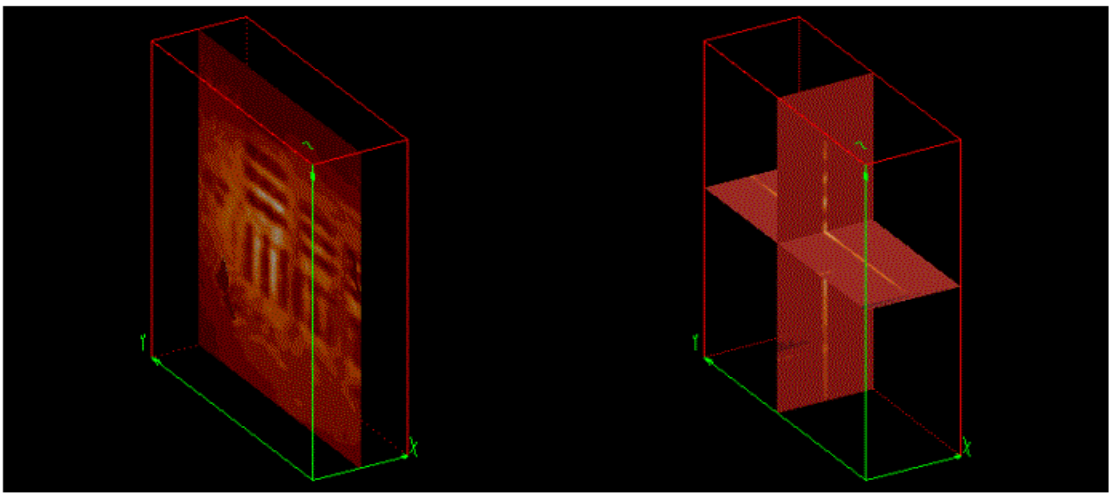

(a) (b)

Figure 5. Holograms of test chart recorded under variable reference delays. (a) hologram in y-z plane. (b) cross section in x-z plane and x-y plane.

2.1.3 Optical Coherence Imaging Applied to Sandstone

2.1.3.1 Sample Preparation and Characterization

The OCI system was initially and successfully used to image to the back of the first layer of grains in a sandstone rock core. Future research using the OCI system to obtain geometric data from sandstone includes performing correlative imaging, i.e., comparing the OCI acquire data to Woods-metal casts of the pore geometry as well as two-dimensional data from scanning electron microscopy (SEM). For this reason, sandstone samples that fit into the SEM system have been used. This report contains the results of the application of OCI to a sandstone sample measuring 25.4 cm by 24.5 cm by 25.4 cm.

Figure 6 shows a direct image of the surface of the sandstone sample taken with an optical microscope at a magnification of 25x. A region of the sample was chosen for interrogation with OCI. This region measures 3.5 mm x 3.5 mm and is represented by the black square in Figure 6. Within the sample region, eight sub-regions (white squares in Figure 6) were selected to acquire 10 sets (labeled as 0001 – 0010) of holograms. The

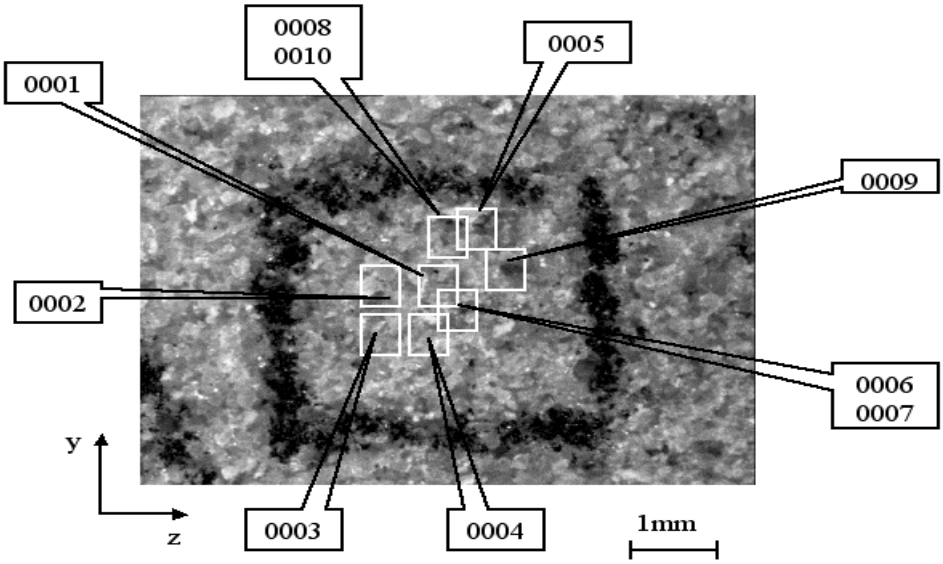

Figure 6. Optical micrograph of the sandstone. The marked areas are the sub-region of OCI data set.

holograms contain images of the coherent light scattered from the sand grains in the sandstone sample. The sample orientation and location in the sample region is determined by comparing the direct image under laser illumination with the incoherent optical micrograph.

For each sub-region, 80 holograms are acquired using the CCD camera. The 80 holograms correspond to increasing depth into the sample, i.e., each hologram is recorded at a different depth within the sample. The sampling depth step size between holograms is 10 μm (microns). The typical image acquisition and transfer time is about 1.5 sec for each image. To increase the signal-to-noise ratio of the CCD camera, 6 frames (230×294 pixels) are averaged in the CCD controller. The exposure time of each frame is 0.06 sec.

Scanning electron microscopy (SEM) was performed on the sandstone sample in the same region as the optical micrograph and the OCI data sets. The SEM image in Figure 7 was acquired using the secondary electron (SE) mode of the SEM with magnification of 50x. The contrast of the SEM image represents surface-tilt, which shows the topology of the surface of the sandstone sample. Although the SEM image can recognize clear surface structure, it cannot get useful information below the surface of the sample.

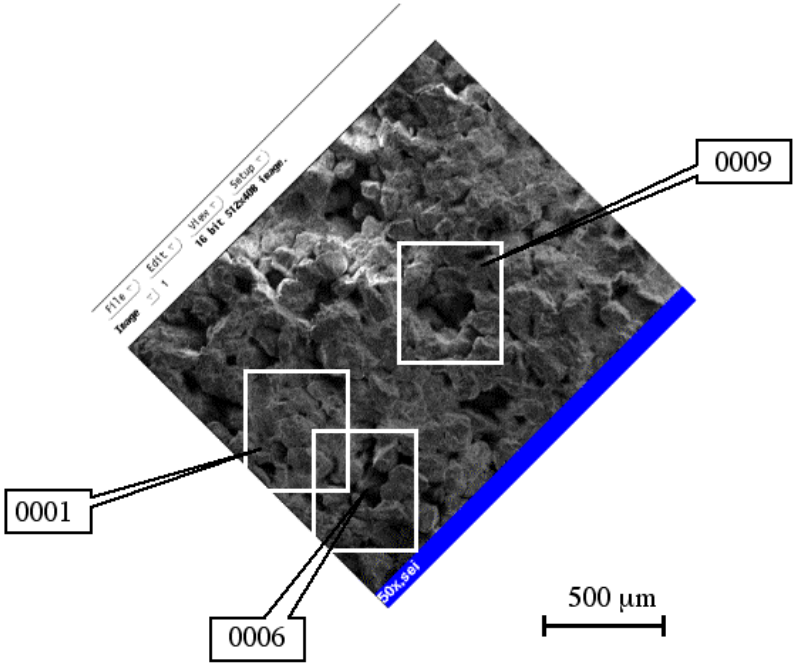

Figure 7. SEM shows topology of the sandstone. The marked areas are the sub-regions of OCI data set in this report, which have same labels as in the optical micrograph.

2.1.3.2 Optimization of the OCI System in the Presence of Background Light

The choice of the intensity of the reference beam is important in order to obtain high contrast in the holograms. For the OCI experiments on sandstone, the incident object beam (probe beam) has a power of 400 mW for a circular region with a diameter of 1.0 mm. The power of the scattering and the ballistic components from the sandstone are about 40 µW, i.e., a difference in power of four orders of magnitude. In the Fourier plane of the 4-F system (Figure 2), about half of the power is cut off by the spatial filter (an optical technique for rejecting scattered light). The reference beam has a power of 300 µW in a circular region with a diameter of 3.0 mm. It is found that the ratio of 1:2 in intensities between signal and reference beams is the best ratio for reconstruction of the holograms of the USAF test chart. However, in the case of sandstone, there are large amounts of incoherent background light (such as scattered light) that can only be partly rejected by the spatial filter. The ballistic components mismatched with the reference beam are also present as incoherent background

light. Therefore, a different intensity ratio is required in the sandstone experiments. In the OCI experiments, an optimized ratio is achieved by synchronously adjusting the reference intensities and the spatial filter.

2.1.3.3 Imaging to the Back of the First Layer of Grains

Figure 8 shows the y-z plane holograms with sampling depth step of 10 μm between the images from the sub-region 0006 in Figure 6 (and also shown in Figure 7). Note that the sampling depth is not equal to true depth in the sample when the light passes through the grains. Assuming the refractive index of the grain in the sandstone is n, the true depth is equal to the sampling depth divided by n inside a single grain. In the case when the light passes through several grains and interfaces between grains as well as the pore structure, the situation is more complicated. It becomes necessary to identify the grain and pore structure before calculating the true depth in the sandstone sample.

In Figure 8, the bright hologram that is observed in image 4 in the marked region (white square) is the top surface of a grain. In the marked regions in images 4 through 12, the bright holograms show different shapes for the different depths. This is caused by the reflections from different facets of the grain.

From the SEM micrograph (Figure 7) and optical micrograph (Figure 6), a surface pore can be seen in the sub-region 0009. Figure 9 shows the holograms around that region obtained using OCI. The squares in the images indicate bright holograms for different sampling depth ranges (i.e., images 6 – 11 and images 11- 19). The bright holograms correspond to the top reflection from different grains near or inside the surface pore according to the comparison between SEM image and optical microgram.

Figure 10 shows the y-z plane holograms of the sandstone for sub-region 0001 in Figure (and also shown in Figure 7) with sampling depth difference of 10 μm between the images. The bright hologram in the marked area (about 100×150 μm^2) in image 1 reflects the top surface of a center grain that is topmost on the sandstone surface in the sub-region. The bright holograms appear again in the same area in the images 21,22,and 23. On the other hand, when looking at the holograms between the top and bottom of the center grain, it should be dark inside the grain area if it has no large defects (microcracks) or voids. The images 9,10,11,12 show the holograms at the sampling depth about 100 μm. The area

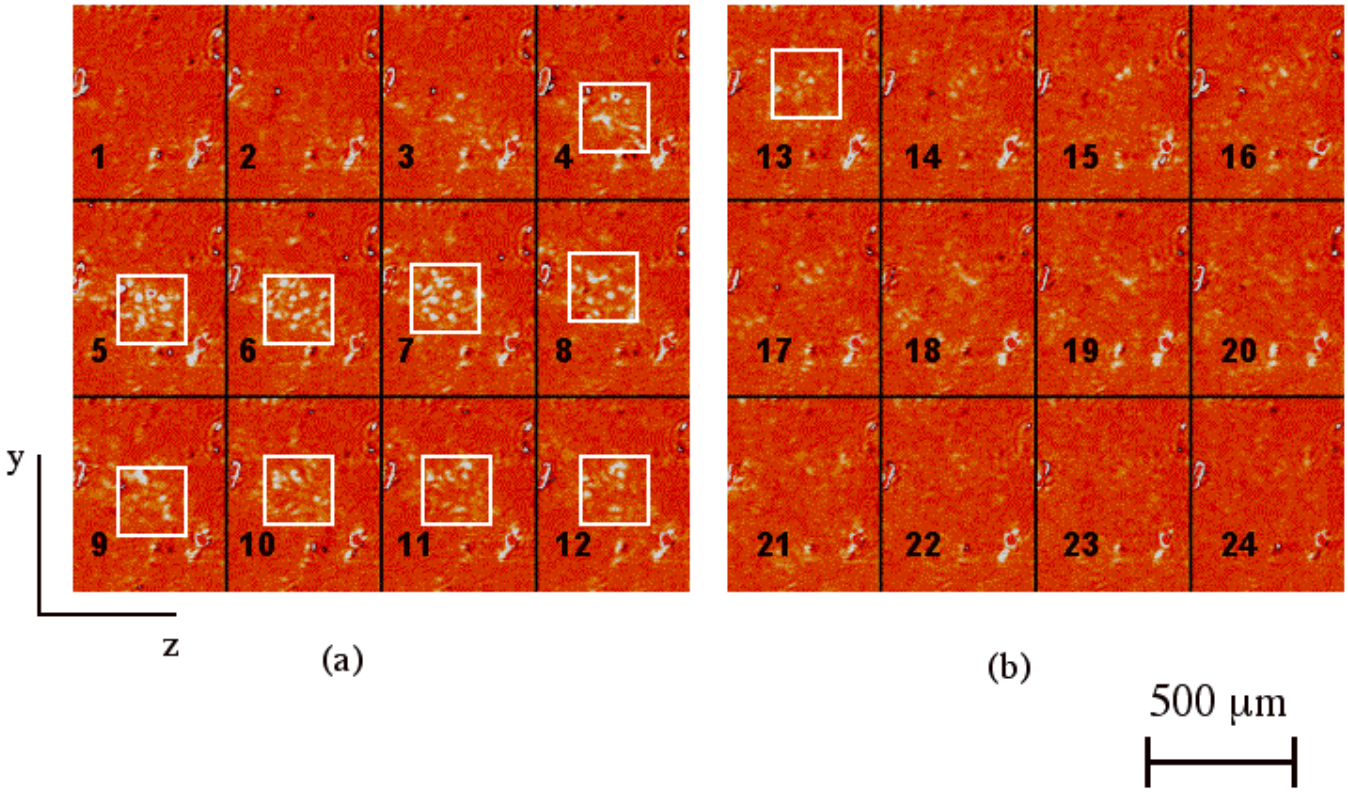

Figure 8. y-z plane holograms recorded at the sub-region 0006 for different sampling depths of 10 μm between the images.

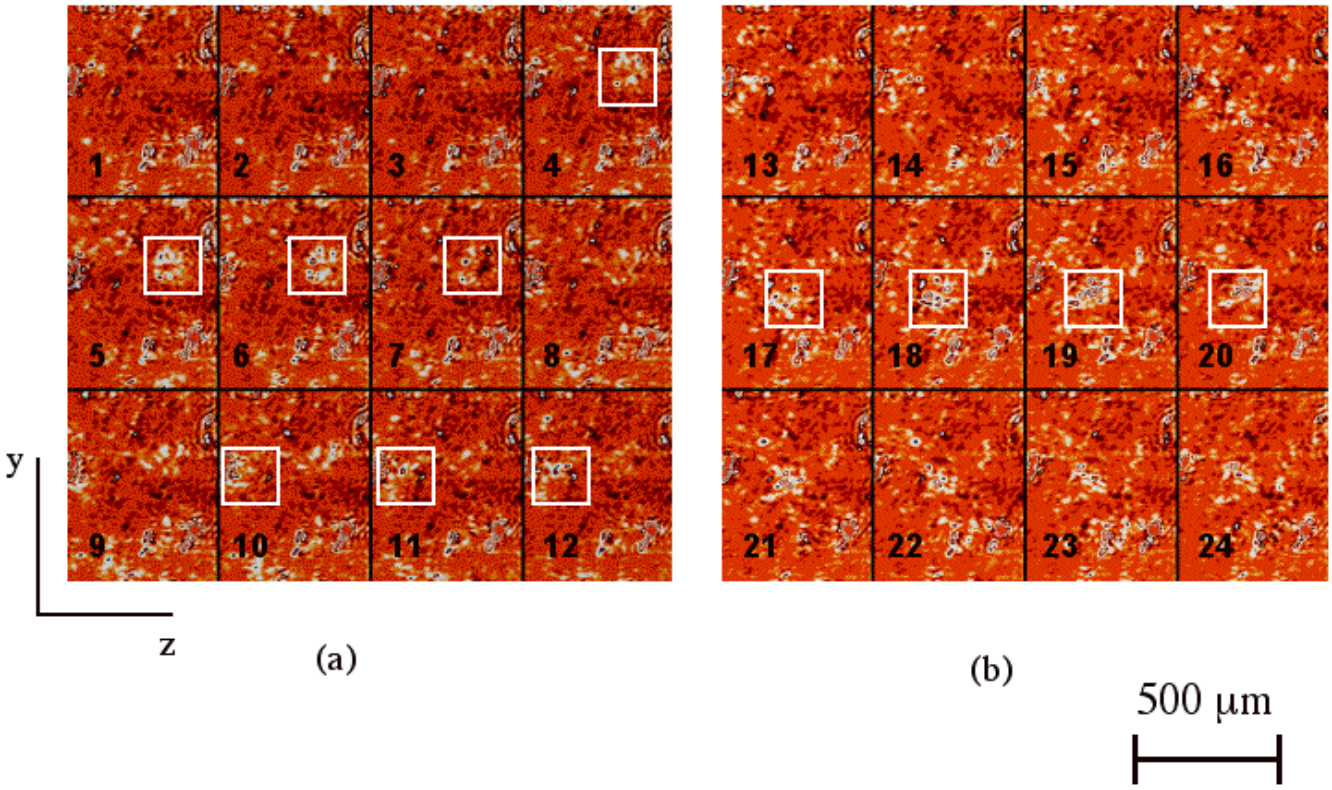

Figure 9. Holograms recorded from top of different grains in the sub-region of 0009. The top difference between image 6 and image 11 is 50 µm, and between image 11 and image 19 is 80 µm.

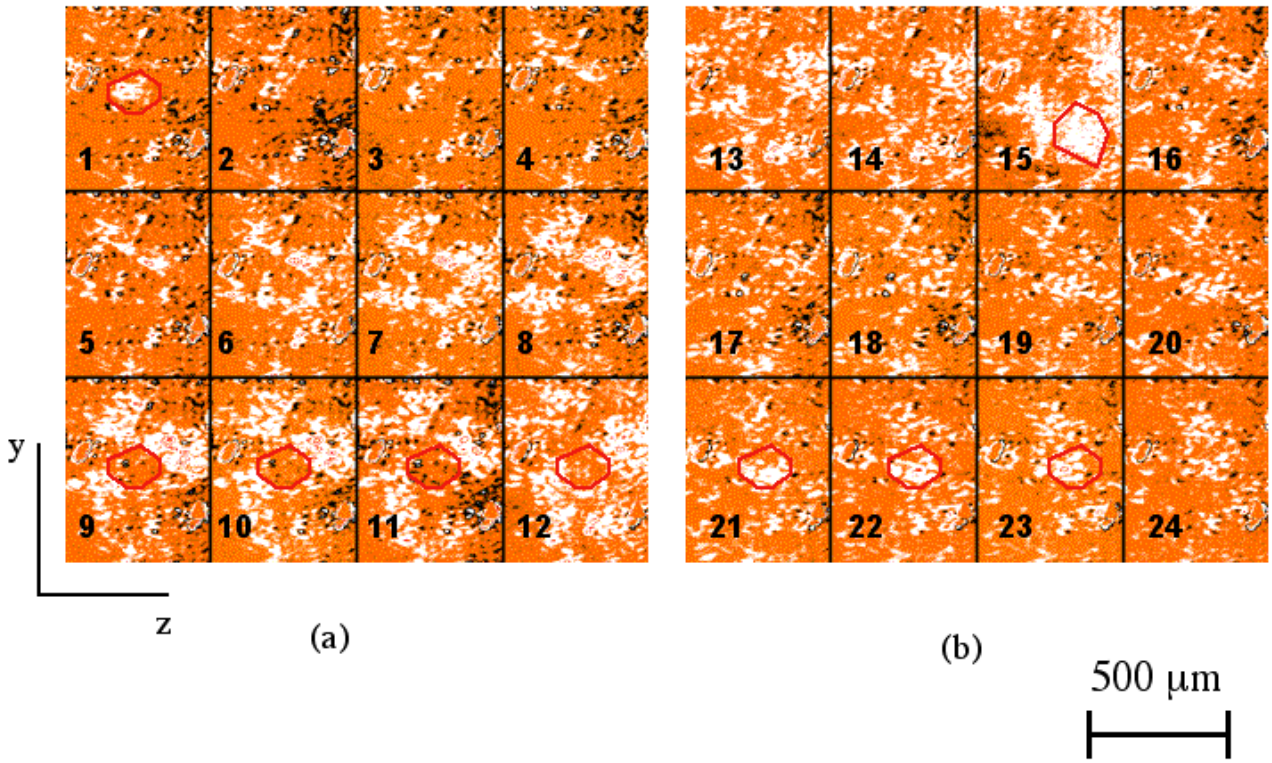

Figure 10. Holograms recorded with different depths from position 0001. The sampling depth between images is 10 μm.

corresponding to the center grain is almost dark (orange color) while the bright holograms (white) of several other grains can be seen in the regions surrounding the marked region. In the center dark area, the lateral shape of the center grain is the same as the grain shape in the SEM image (Figure 7) for the same sub-region. Therefore, the bright holograms inside the marked area in images 1 and images 21,22,23 are from the top and bottom of the grain, respectively. If the refractive index of the grain in the sandstone is about 1.5, then the thickness of the grain is approximately 150 μm. The center grain can be observed in the cross section in x-z plane as shown in Figure11. It is interesting to point out that except for the top and bottom facets of the grain, at least one tilted facet can be seen at the side of the grain in the cross section image (upper left region of the region outlined with the thin red

line). Several bright columns along the x-axis can be seen at the top and bottom of the reconstructed depth cross-section Figure 11. Because these features exist for all depths at the same location, these features are not holograms of the sandstone. These columns are from scattered light from scattering centers in the PRQW holographic film.

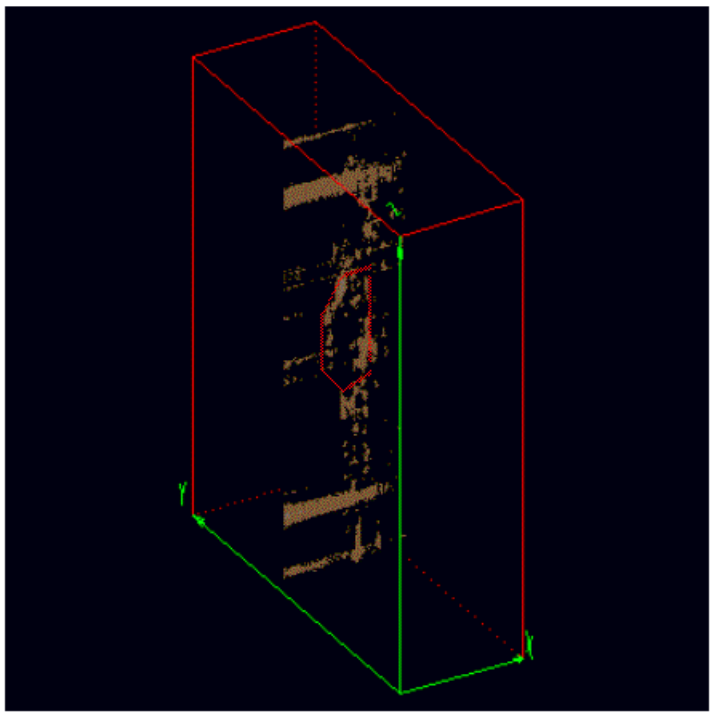

Figure 11. x-z plane hologram shows cross section of the grain.

2.2 MICRO-MODELS

2.2.1 Construction and Installation of Equipment

2.2.1.1 Lithographic Facilities

During the initial months of this project we initiated a major upgrade of our lithographic facilities. Our micro-models are constructed using the two types of optical lithography shown in Figure 12. This section gives a brief description of the procedures for performing

optical lithography; complete details are given in the manufacturer's manual (Shipley, 1982) and by Thompson, Willson and Bowden (1994).

In optical lithography a pattern is transferred using a visible light image to a photo-sensitive polymer layer called photoresist. This layer acts essentially as photographic film. When a region of the photoresist is exposed to a sufficiently large integrated intensity of blue light, a photochemical reaction within the photoresist makes the region soluble in a special developer solution (usually just a base). The unexposed photoresist is not soluble, so after development the photoresist layer contains a negative image of the original light pattern. In all of our work we have used Shipley photoresist types 1805 and 1827, and their standard developer (Shipley, 1982). The image has been transferred to the photoresist in two different ways. In one method (Figure 12, left) a photomask is put in direct contact with the photoresist and the exposing light is transmitted through the mask. This mask is typically an opaque metal layer on a glass substrate, or a small portion of an ordinary video transparency sheet onto which the appropriate pattern has been printed. With this contact configuration the mask pattern is transferred in a 1:1 fashion to the photoresist sample; i.e., without magnification or reduction in size. We use this method for making the coarse (i.e., largest scale) features of the micro-models. The smallest sample features are made by projecting the mask pattern onto the photoresist through a microscope objective. We employ a specially modified optical microscope which enables the image of the mask to be focused onto the sample at the same time as the sample is in focus to the observer. Projecting through a 50x objective yields a 50:1 reduction in the size of the image relative to the scale of the mask. In this way we can routinely achieve sub-micron feature sizes at the sample.

Construction of a complete micro-model involves several steps (Figure 13). The first is to transfer the pattern of the desired flow geometry into a photoresist layer – this is accomplished using optical lithography as just described. The resulting glass substrate/photoresist layer will form the bottom and sidewalls of the final micro-model. The top wall (ceiling) of the micro-model is formed by a second glass coverslip. This "top plate" is bonded to the bottom layer using another layer of photoresist – this bonding is

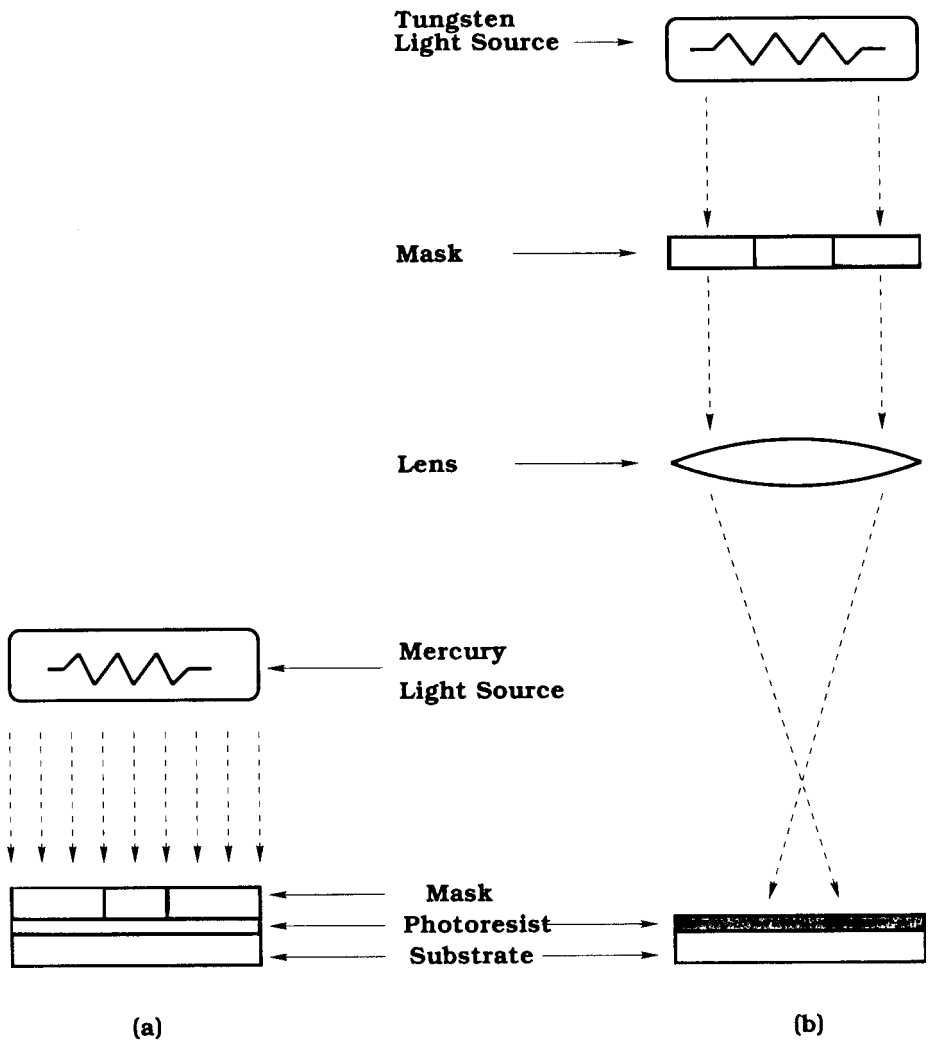

Figure 12: Schematics of the procedures used for optical lithography. Left: contact lithography. Right: projection lithography.

accomplished by bringing the two glass coverslips into contact with gentle pressure (approximately 1 atm, applied in a special holder in which a flexible plastic sheet is pulled against the sample by an applied vacuum) immediately after application of photoresist to the top plate (Figure 13a). The top plate also contains two holes (approximately 1 mm in diameter, drilled ahead of time) that serve as inlet and outlet for the finished micro-model (Figure 13c). The inlet and outlet regions are fairly open spaces (approximately 4 mm on a

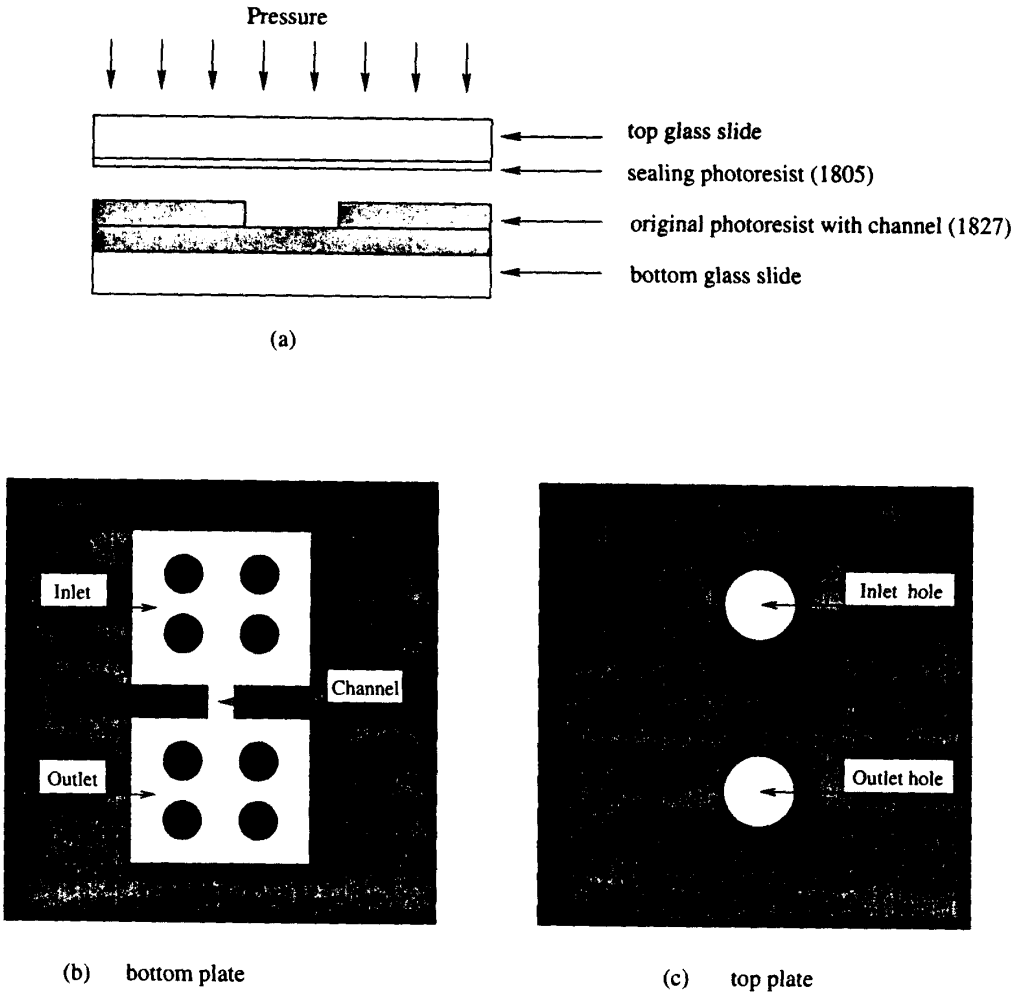

Figure 13: Micro-model layout. (a) Side view showing bottom plate containing micro-model pattern and top plate just prior to bonding. The glass slides are cover glasses 200 microns thick. The photoresist layers are 0.5 micron (type 1805 photoresist) and 2.7 microns (type 1827 photoresist). (b) Arrangement of inlet, outlet, and sample (channel) regions. (c) Inlet and outlet holes are drilled in the top plate.

side) on the micro-model, and contain “pillars” which are approximately 0.5 mm in diameter to prevent collapse of the structure (Figure 13b). The working region of the micro-model is the area labeled as “channel” in Figure 13b. This is where a percolative pattern is created in the bottom photoresist layer.

During the initial months of this project we performed a major upgrade of our lithography laboratory. This laboratory now has three “clean benches” in which all sample processing is carried out. The clean benches are laminar flow hoods in which a constant upwards flow of filtered air is maintained. This ensures that dust and other airborne contaminants do not come into contact with our samples prior to final bonding of the coverplate. In our old

laboratory set-up, samples were handled “in the open” and were not protected from airborne particulates. This was a problem, since dust particles that became attached to the sample surfaces prior to bonding caused the bonds to leak, resulting in un-useable samples. The new clean benches have reduced our problems with airborne particulates, greatly improving our yield of good samples (our current yield is 75%, as compared to 25% in the old laboratory). This improved yield enables us to fabricate more complicated flow patterns with acceptable success rates, and also improves the optical quality of the micro-models – this is crucial for reasons that will be described below.

2.2.1.2 Flow Measurement Apparatus

A schematic of our measurement apparatus is shown in Figure 14. This apparatus is used for simultaneous measurements of flow rate and optical characterization of the geometries of the various phases within the sample. This apparatus was constructed during the initial months of this project – the design is similar to an older setup that was used for studies of single phase flow. The main improvements are (1) the addition of a second pressure sensor, so that both the input and output pressures can be measured (in the old setup the outlet pressure was always atmospheric pressure), and (2) the installation of a new video camera interfaced to an optical microscope.

The new apparatus enables multiphase flow to be studied as follows. The micro-model is initially saturated with a fluid such as silicone oil, which is inserted through the “outlet” region in Figure 14. A second fluid, such as nitrogen gas, is then introduced through the inlet region. The flow rate of this second phase is measured using video microscopy together with an “on-chip” flow capillary. This capillary is a long narrow flow channel that is arranged to be in series with the sample and is located between the sample and the outlet region, as shown in Figure 15. The meniscus of the second fluid is tracked via microscopy as it moves along the measurement capillary, and the flow rate calculated from the known dimensions of the capillary (typically 0.2 mm wide and 2.7 microns deep). This method makes it possible to measure extremely small flow rates very quickly. All measurements are conducted at room temperature (temperature stability better than 0.5 degree Celsius during a measurement), with the apparatus located within one of the clean bench environments.

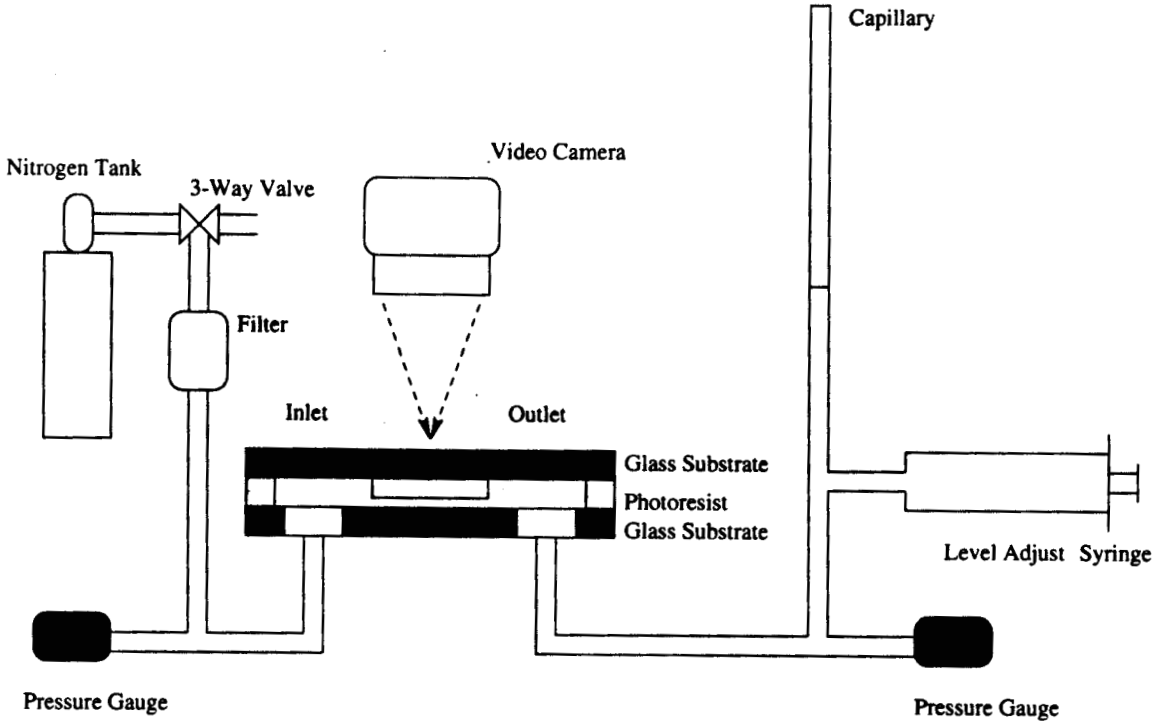

Figure 14: Apparatus used for measurement of flow rates and imaging of fluid geometry within a micro-model. The pressure sensors are piezoelectric sensors (model PX550C1 from Omega Engineering). The video camera system is a SPOT-1 RT color system (Diagnostic Instruments, Inc.) interfaced to a Macintosh G4 computer.

The measurement of *IAV* is also accomplished with our video microscopy setup. For this we capture the image of the micro-model and do image processing with the computer interfaced to the camera. A captured image for a sample containing two fluid phases is shown in Figure 16; the images are taken in red light, as blue light causes unwanted photochemical reactions in the photoresist (Thompson, Willson, and Bowden, 1994). This is a nonrandom micro-model that was designed to test our fabrication and image analysis procedures. The squares are photoresist obstacles (i.e., regions inaccessible to the fluids), the brightest red region is occupied by silicone oil, and the region of intermediate color is filled with nitrogen gas. In this experiment the micro-model was initially filled with oil, which was then displaced with nitrogen. Interestingly, a pocket of oil was trapped within the structure, and was not expelled by the gas. The image quality and in particular the consistency of the brightness and color are seen to be quite good. This makes it possible to use image analysis

software to obtain accurate values for the areas occupied by both fluids and the interfacial area, both of which are crucial for our studies.

2.2.1.3 System Testing

The fabrication and measurement facilities described above were tested by preparing micro-models of various geometries, including the nonrandom pattern in Figure 16, and other samples described in the next section. The sample yield of 75% noted in section 2.1.1 indicates that our new lithography laboratory is a significant improvement with respect to our previous lab. Another excellent test is the optical quality that can be obtained in our imaging.

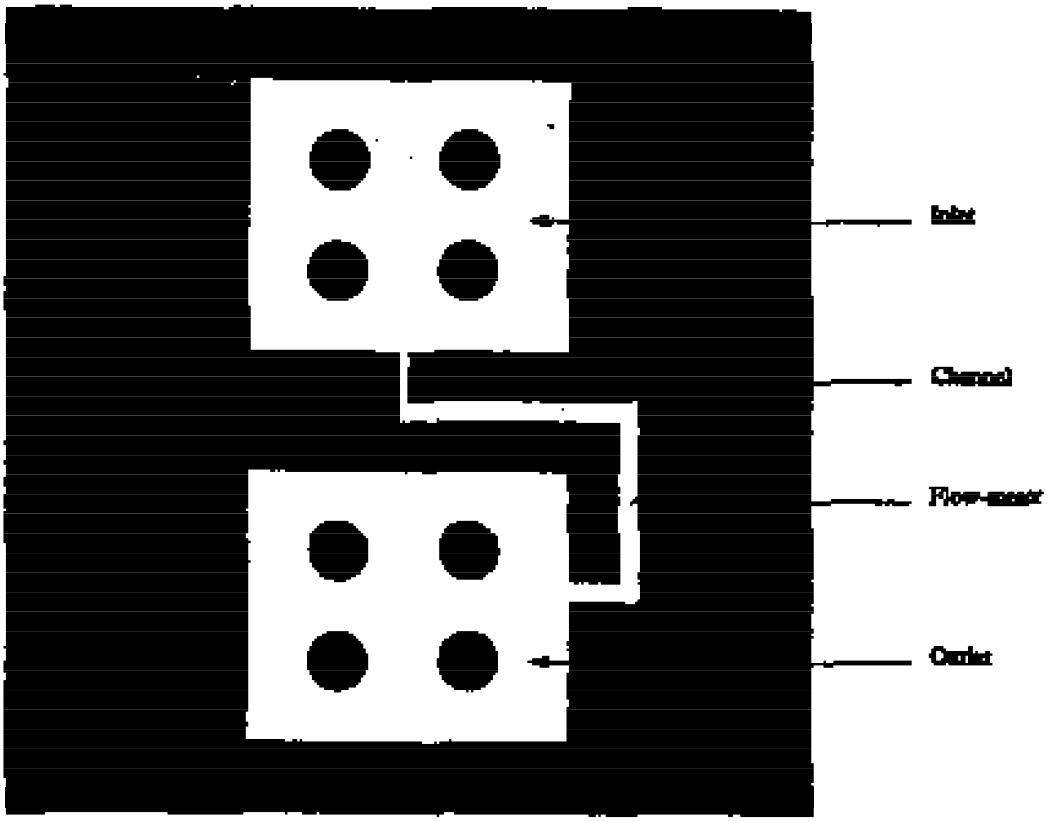

Figure 15: Micro-model with an "on-chip" capillary for the measurement of flow rates. The percolative flow structure is located in the region labeled “channel.”

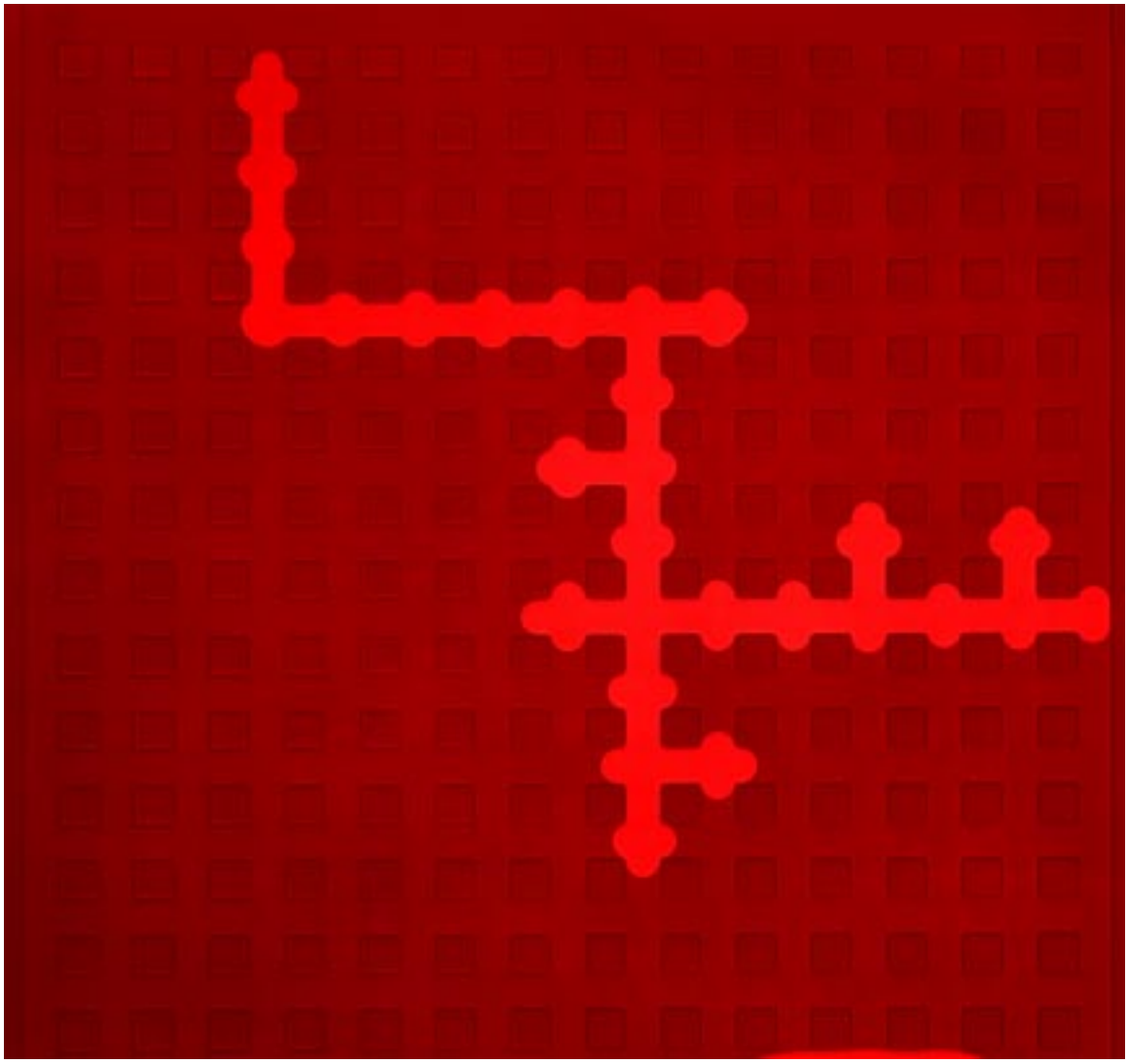

Figure 16 : Nonrandom micro-model containing silicone oil (bright red) and nitrogen gas. See text for explanation.

Figure 17 shows a brightness histogram for a random micro-model (see Figure 19) containing only nitrogen gas. The histogram has a large peak at brightness levels below 50 (in the arbitrary units used to measure brightness) corresponding to the photoresist regions (which are inaccessible to fluid) and another peak near 100 corresponding to the open region which here was filled with nitrogen gas (the increase at 250 is an artifact due to the edge of the image and can be easily disposed of in the final analysis). The key point here is that the open and closed regions are well separated in their brightness values, so that an accurate automated measurement of saturation and also the interfacial area separating the two regions can be performed. This analysis, and the calculations of *IAV* were performed with the IDL software package version 5.3, from Research Systems, Inc.

2.2.2 Experimental Results

2.2.2.1 Studies of Multiphase flow

An objective of this project is to test upscaling theories for relative permeability. One way to carry out such a test is to compare the behavior of micro-models with that of a real porous material. In our work we wish to compare with sandstone as studied in the Wood's metal task of this project. Hence we need to prepare micro-models that are statistically similar to the pore geometry found in sandstone. Figure 18 is an SEM (scanning electron microscope) micrograph of the pore structure of a sandstone sample. The image was taken using the SEM in the backscattered mode to image the different materials filling the pore space. In the figure, the pores are represented by the white and gray regions. The black regions represent the matrix of the sandstone. The image illustrates the complexity of the pore geometry in sandstone. The pore space is unconnected in the image, i.e., a continuous path for fluid flow is not observed in any direction in this two-dimensional image. Fluid flow through sandstone is a three-dimensional problem because it is the third dimension that enables the connection of pores to form a flow path. A challenge of this project is comparing the hydraulic properties from the two-dimensional (2-D) micro-models to the hydraulic properties from the three-dimensional (3-D) sandstone cores. There is no known rigorous

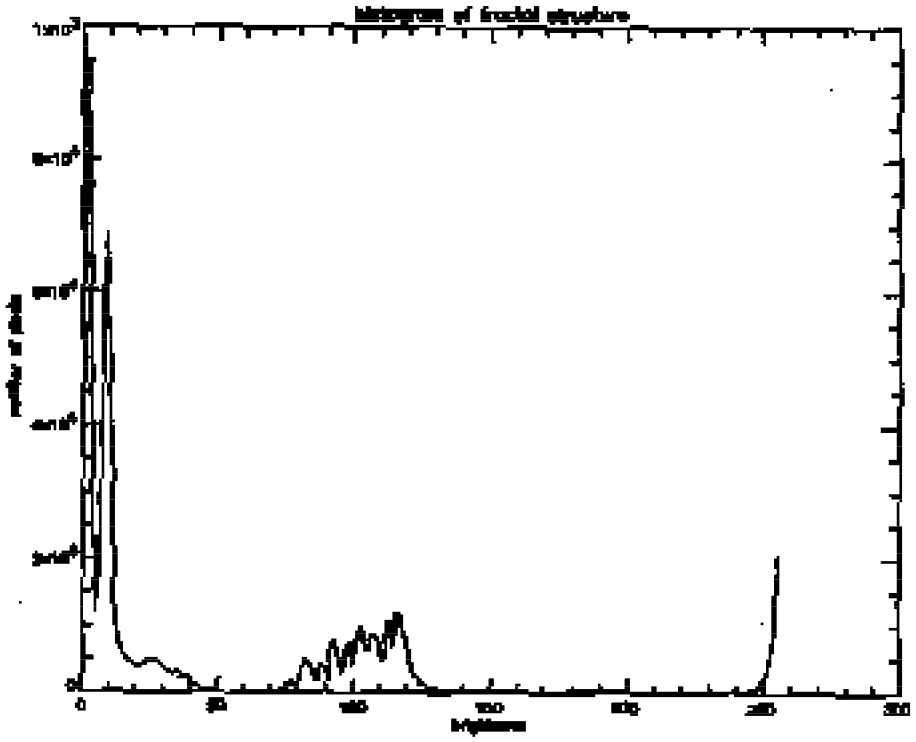

Figure 17: Brightness histogram of the micro-model in Figure 19 when filled with nitrogen gas. See text for discussion.

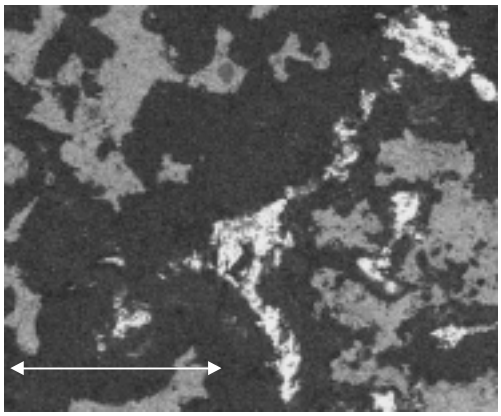

Figure 18: An image of the pore geometry in sandstone obtained from scanning electron microscopy. The sample has been injected with Wood's metal (white regions) and epoxy (gray regions). The black regions represent the matrix of the sandstone. The arrow in the image represents 500 microns.

formalism for scaling between different dimensionalities. We will attempt to link the 2-D and 3-D information in an approximate manner using a percolation approach.

The percolation threshold P_c is the concentration of open pore space at which a fully connected open region that spans the entire sample is first formed. Flow is only possible when the concentration of open pore space P is greater than or equal to P_c. The value of P_c depends on the dimensionality and structure of the system. Since the micro-models are 2D while sandstone is 3D it is not meaningful to compare the two at the same value of P. It makes more sense to compare the two types of samples if they have the same value of P- P_c , since they are then the same distance from P_c , i.e., the same distance from the onset for flow.

In a 3D close packed structure (as appropriate for sandstone) the theoretical value is P_c = 0.18 (Stauffer and Aharony, 1992). The porosity of the sandstone was measured using a wet/dry method. In the wet/dry method, the sample is vacuum saturated and the weight difference before and after saturation is used to calculate the porosity. The porosity of ten sandstone samples is approximately 19.25% $\pm$ 0.11%. Hence they are approximately 1% above the percolation threshold. We therefore constructed our micro-models to have P- P_c = 0.01. We first determined P_c by making a series of samples of different P using the one tier fractal geometries described by Nolte and Pyrak-Nolte (1991), and measuring the value of P at which flow first appeared. The measured value of P_c was 0.51 $\pm$ 0.01 which is very close to the expected value of 0.50 (Stauffer and Aharony, 1992).

Figure 19 shows a micro-model with a geometry specified by the one tier model of Nolte and Pyrak-Nolte (1991), with a value of P which is 1% above the percolation threshold. This photo was taken with the sample filled with nitrogen gas. The light colored regions are the gas (i.e., open pore space) and the dark regions are the photoresist (inaccessible to fluid). Figure 20 shows the same micro-model after silicone oil had been forced into the model with pressure. The brightest region is again nitrogen, the darkest region is the photoresist (i.e., inaccessible to fluid) and the region of intermediate brightness is oil. It is seen that pockets of gas have been trapped within the oil, and the geometry of the gas filled region appears to be fractal. The fluids used in this experiment were silicone oil and nitrogen gas. Their properties are listed in Table 2.

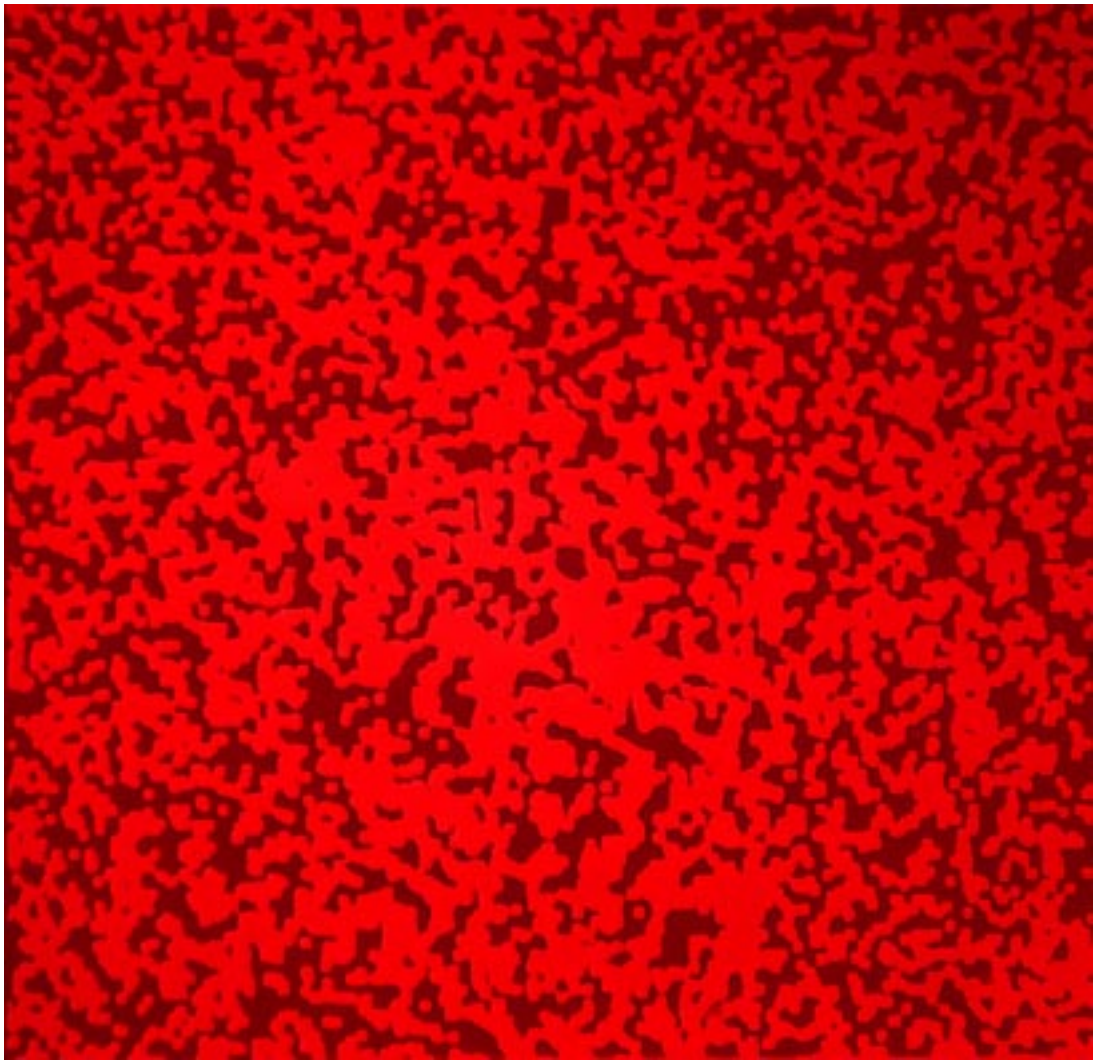

Figure 19: Micro-model designed after the measured pore geometry of sandstone. The field of view is approximately 0.6 mm across.

Table 2: Properties of silicone oil and nitrogen gas. The surface tension of silicone oil is given relative to nitrogen gas.

fluid	density	viscosity	surface tension
silicone oil	0.964 g/cc	101.8 centipoise	20.9 mN/m
nitrogen gas	1.251 g/liter (1atm)	175 micropoise (@25C)	----------

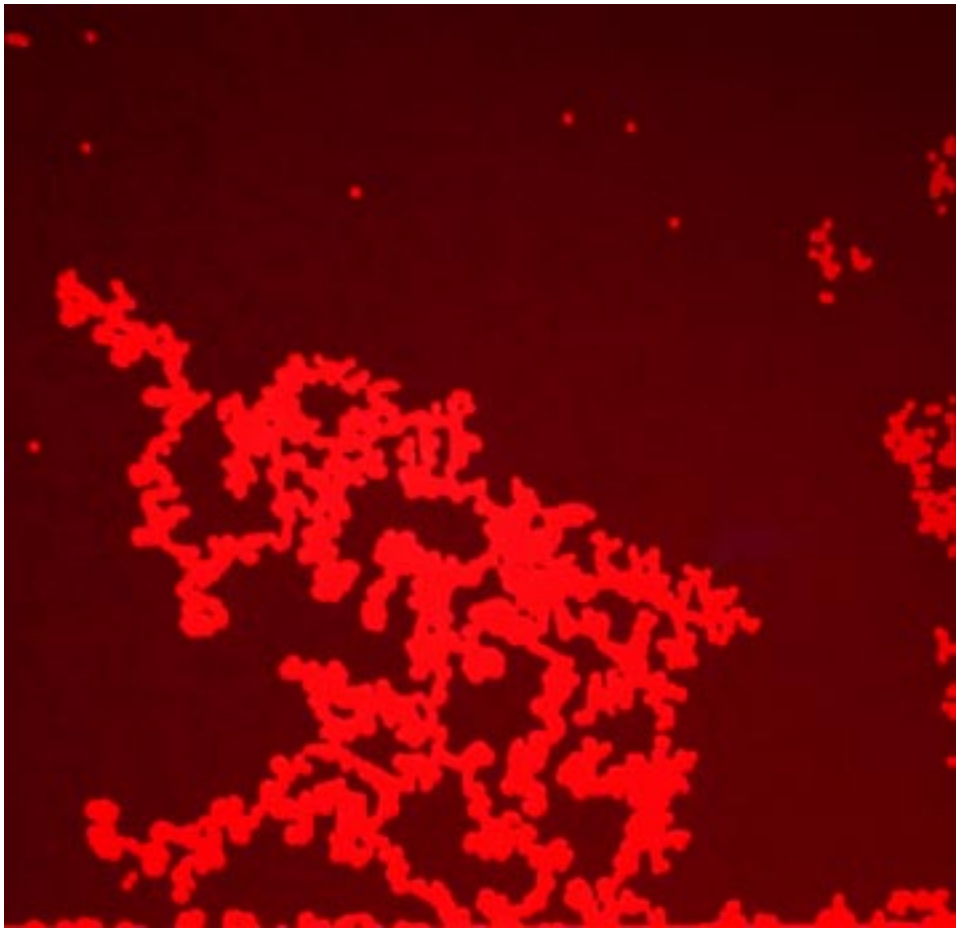

Figure 20: Micro-model of Figure 19 filled with nitrogen gas (brightest regions) and silicone oil (regions of intermediate color).

The photo in Figure 20 shows the system after it had been allowed to come into equilibrium at a particular value of pressure (P_{cap}) and flow rate (of the oil, Q). This equilibration process took several minutes; the system was then stable as long as the pressure was held constant. We then also measured the saturation of oil, S, and the interfacial area per unit volume, IAV. Note that this is the area of the interface separating the oil and gas filled regions. Since we are in 2D the IAV is actually the line length of this region normalized by the area of the entire sample. Results for these two quantities as functions of the pressure are shown in Figures 21 and 22. Both quantities are seen to trace out hysteresis loops, indicated by the arrows, as the system is drained and then re-filled, starting from point A in the figures.

By performing the drainage-imbibition cycle many times (Figures 21 and 22 are one typical cycle), we found that the precise trajectory followed by the system in P_{cap}-S-IAV

space depended on the speed with which the pressure was changed when going from point to point within a cycle.

A key claim of recent theories of multiphase flow is that *IAV* is effectively a state variable and is therefore essential in any description of the flow. At present the theoretical arguments are quite general and based on conservation laws and volume averaging. There do not yet exist quantitative theoretical predictions for the P_{cap}-*S*-*IAV* function for any real system. However, we can still make a strong test of the theory by considering the form of the measured P_{cap}-*S*-*IAV* surface. Specifically, we ask if this surface is single valued. Figure 23 shows results for silicone oil/nitrogen gas in the micro-model of Figure 19. We find that the *IAV* function is indeed single valued. For a given value of P_{cap} and *S*, the value of *IAV* is unique, even if this point in P_{cap}-*S* space is arrived at indifferent ways (along different trajectories). This is a crucial confirmation of the theoretical importance of *IAV*. We should note that our finding is similar to that found in a numerical study of a network flow model (Reeves and Celia, 1996), who also found that the *IAV* surface was single valued.

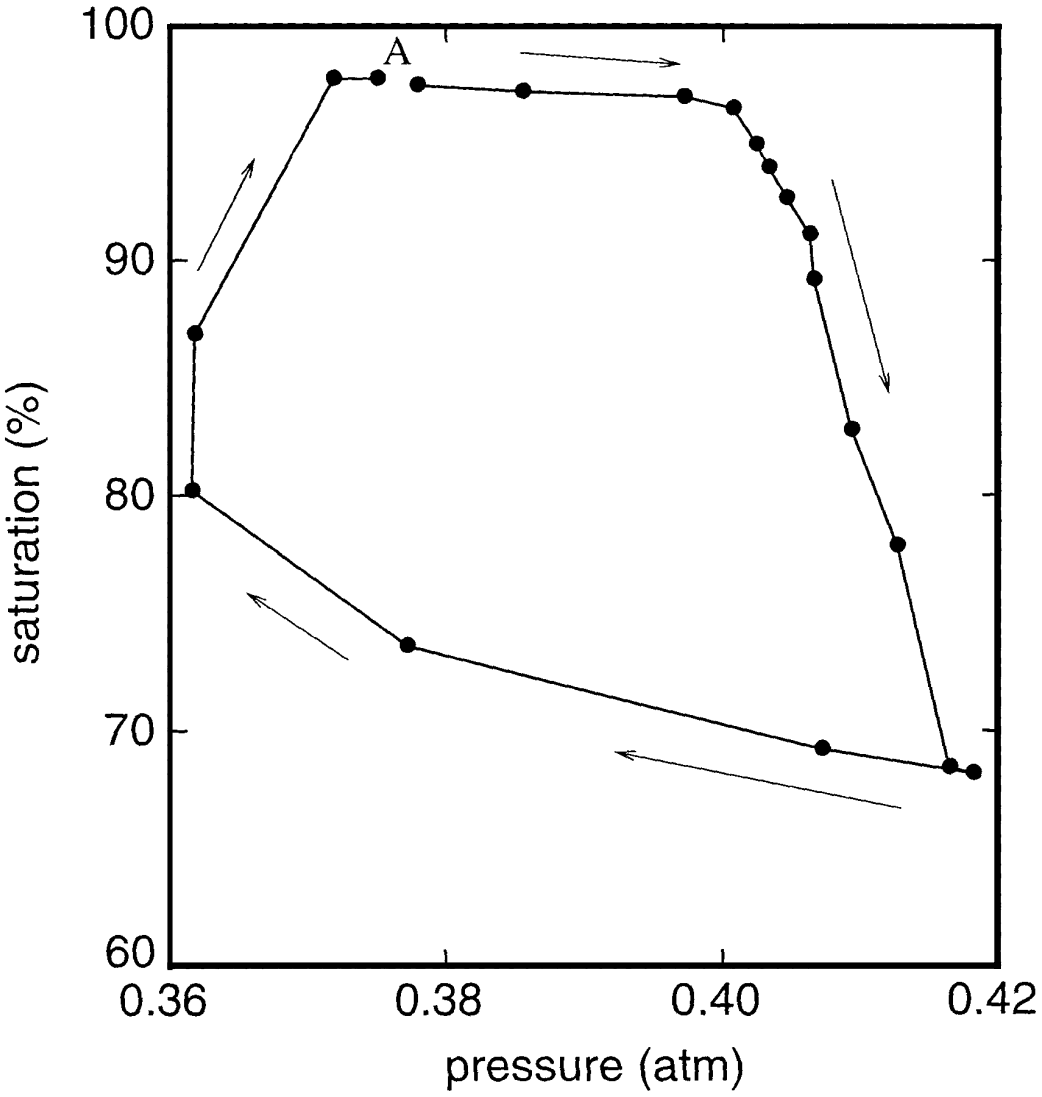

Figure 21: Saturation (volume fraction of oil) as a function of pressure, as the system is first drained, and then re-filled with oil.

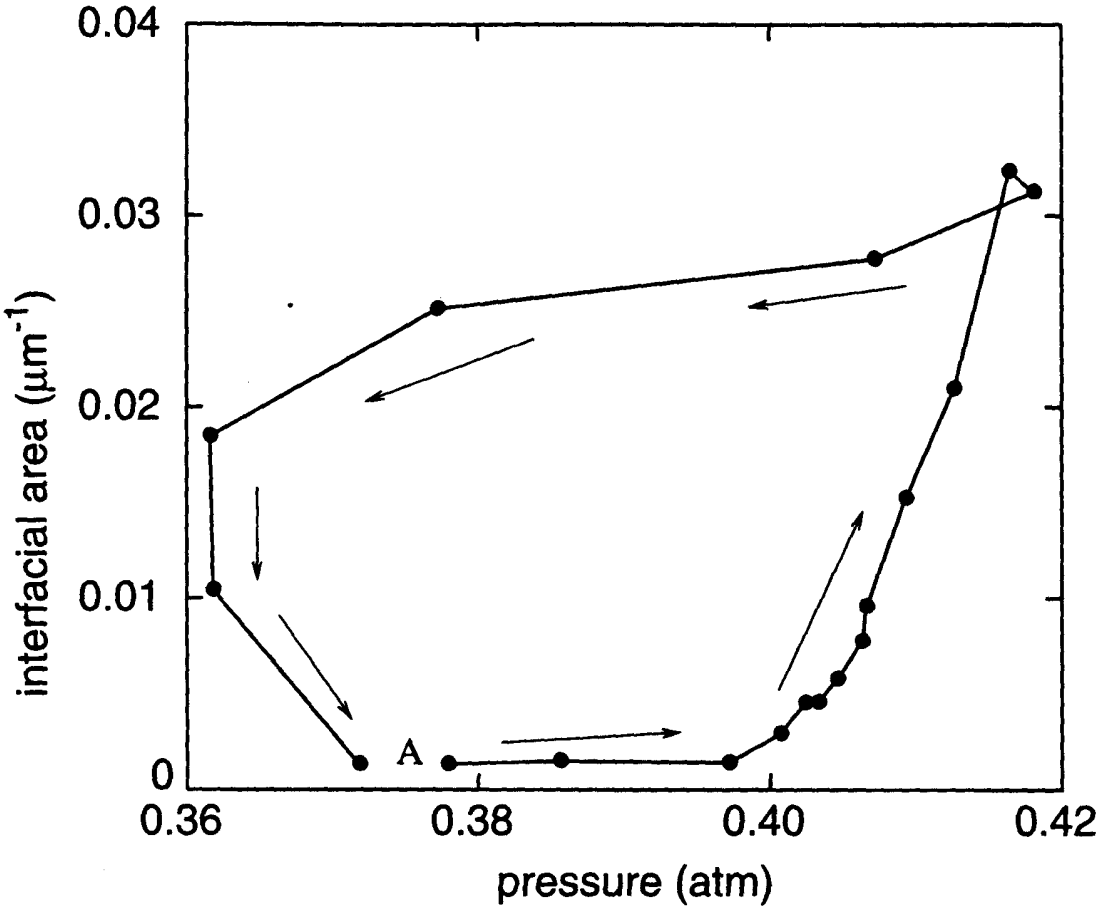

Figure 22: IAV (in this 2D sample this quantity actually the interfacial perimeter length divided by the area of the sample) as a function of pressure as the micro-model is first drained, and then re-filled with oil.

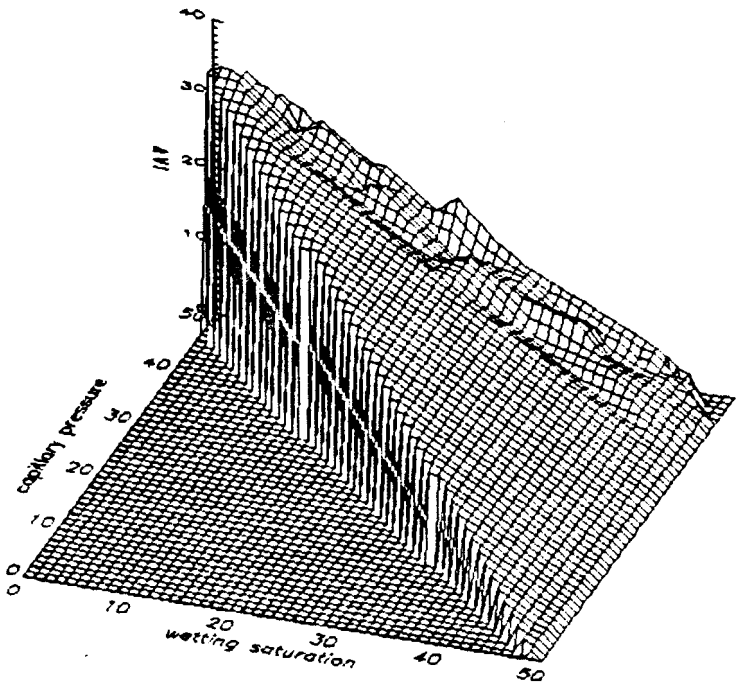

Figure 23: P_{cap}-S-IAV surface. See text for discussion.

3.0 Conclusions and Future Work

3.1 Optical Coherence Imaging

The milestone was achieved by imaging to the back of the first layer of grains in a sandstone sample. This work represents the first demonstration that Optical Coherence Imaging (OCI) can image into rock. The acquired OCI holograms (i.e., data) provide information on the thickness of the grain (from reflections from the top and bottom surfaces of the grains) as well as information on the geometry of the grains (from reflections from some of the side facets of the grains). The deepest information, according to our data sets, can be achieved for about 400 _m underneath the surface of the sample. Calibration of the OCI system showed that the lateral resolution of the holograms is 10 μm while the depth

resolution is about 30 μm. The lateral resolution is set by the choice of optical lenses, and the dependence of diffraction efficiency on the fringe spacing. The depth resolution is fixed by the coherence length of the laser.

The next step in the development of OCI for imaging into sandstone samples requires the following future work:

1. In our experiments, the limitation of the dynamic range of the cooled CCD camera is from the scattering centers in the PRQW device. In principle, if the integration time of the cooled CCD camera is increased, more grains can be detected beneath the surface of the sandstone. In future work, we will increase the capability of OCI imaging into the sandstone by preparing scattering free PRQW devices.

2. Since the intensity ratio is important to get good hologram contrast. It is necessary to quantitatively determine the optimal intensity ratio between the signal arm and reference arm compared with theoretical analysis.

3. The use of index matching liquids will reduce the reflection from the top surface of the sandstone as well as from interfaces inside sandstone. This will enable the OCI imaging system to probe deeper into the sample.

4. To improve the interpretation of the OCI holograms, experiments will be performed where ink is injected into the sandstone sample. The ink will block reflections from deep within the sample. This will enable delineation of the pore structure within the sample and a validation of interpretation of the OCI holograms.

5. The OCI images of the grain structure and pore structure will be compared with the same data obtained using measurements from the Wood's metal injection Task which is part of this contract.

6. Finally, the Wood's-metal-injected sandstone will be subjected to hydrofluoric etching. This will remove the sandstone grains from the sample and leave a free-standing Wood's metal cast of the pore structure. The OCI system will be used in the laser ranging mode to measure the pore shape. This data will be compared to the holograms of the pore structure obtained from imaging through the grains of the sandstone.

3.2 Micro-Models

We have obtained the first experimental results for the P_{cap}-*S*-*IAV* relation, and have found that *IAV* is a single valued function of capillary pressure and saturation. This is the first experimental test of the theories that predict the importance of *IAV*. The next key test of the theory will be to check if it can predict the quantitative functional form of the P_{cap}-*S*-*IAV* surface. We therefore plan to make much more extensive measurements of this surface, in a variety of micro-model geometries and with other fluids.

Our measurements of *IAV* have so far all been with zero flow. When filled with silicone oil/nitrogen gas, it is only possible to trace a trajectory in P_{cap}-*S* space with zero flow. Once the gas flow rate becomes non-zero, the value of P_{cap},*S,* and *IAV* cease changing. For the future we will attempt to overcome this problem by studying other combinations of fluids, especially ones with a lower viscosity that silicone oil

4.0 References

Darcy, H., Determination of the laws of flow through sane, Les fontaines publiques de la ville de Dijon, Victor Dalmont, Paris, 1856, 590-594, (translated and reprinted in Physical Hydrology, edited by R. A. Freeze and W. Back, Hutchinson Ross Publishing Company, Stroudsburg, PA, 1983).

Giordano, N., and J. T. Cheng, Microfluid mechanics: Progress and opportunities, J. Phys. Condensed Matter., accepted for publication (2001).

Gray, W. G., General conservation equations for multi-phase systems: 4. Constituitive theory including phase change, Adv. Water Resources **6**, 130-140 (1983).

Hassanizadeh, S. M. and W. G. Gray, General conservation equations for multi-phase systems: 1. Averaging procedure, Adv. Water Resources **2**, 131-144 (1979).

Hassanizadeh, S. M. and W. G. Gray, Mechanics and thermodynamics of multiphase flow in porous media including interphase boundaries, Water Resource Research **13**, 169-186 (1990).

Hyde, S. C. W., R. Jones, N. P. Barry, J. C. Dainty, P. M. W. French, K. M. Kwolek, D. D. Nolte and M. R. Melloch, Depth-resolved holography through turbid media using photorefraction, IEEE J. Sel. Top. Quant. Electron. 2, 965 (1996).

Izatt, J. A., M. D. Kulkarni, K. Kobayashi, M. V. Sivak, J. K. Barton and A. J. Welch, Optical Coherence Tomography, Optics and Photonics News (May, 1997).

Izatt, J. A., M. D. Kulkarni, H.-W. Wang, K. Kobayashi and M. V. Sivak, Optical coherence tomography and microscopy in gastrointenstinal tissues, IEEE J. Sel. Top. Quant. Electron. 2, 1017 (1996).

Jones, R., N. P. Barry, S. C. W. Hyde, P. M. W. French, K. M. Kwolek, D. D. Nolte and M. R. Melloch, Direct-to-Videa holographic readout in quantum wells for 3-D imaging through turbid media, Opt. Lett. 23, 103 (1998).

Jones, R., S. C. W. Hyde, M. J. Lynn, N. P. Barry, J. C. Dainty, P. M. W. French, K. M. Kwolek, D. D. Nolte and M. R. Melloch, Holographc storage and high background imaging using photorefractive multiple quantum wells, Appl. Phys. Lett. 69, 1837 (1996).

Kalaydjian, F., Origin and quantification of coupling between relative permeabilities for two-phase flow in porous media, Transport in Porous Media **5**, 215 (1990).

Lenormand, R., C. Zarcone, and A. Starr, J. Fluid Mech. **135**, 337 (1983).

Lenormand, R., and C. Zarcone, Transport in Porous Media **4**, 599 (1989).

Muccino, J. C., Gray, W. G. and L. A. Ferrand, Toward and improved understanding of multiphase flow in porous media, Rev. Geophys. **36**, 401 (1998).

Nolte, D.D, and L. J. Pyrak-Nolte, Stratified continuum percolation: Scaling geometry of hierarchical cascades, Phys. Rev. A **44**, 6320 (1991).

Nolte, D. D., Semi-insulating Semiconductor Heterostructures: Optoelectronic Properties and Applications, J. Appl. Phys., 85, 6259 (1999).

Pan, Y., E. Lankenau, J. Welzel, R. Birngruber and R. Engelhardt, Optical coherence gated imaging of biological tissues, IEEE J. Sel. Top. Quantum Electron. 2, 1029 (1996).

Reeves, P. C. and M. A. Celia, A functional relationship between capillary pressure, saturation, and interfacial area as revealed by a pore-scale network model, Water Resource Research **32**, 2345 (1996).

Shipley Co., Microelectronic Product Guide, Newton, MA, 1982.

D. Stauffer and A. Aharony, Introduction to percolation theory, Taylor and Francis, London ; 1992.

Soll, W. E., M. A. Cella, and J. L. Wilson, Water Resource Research **29**, 2963 (1993).

Tearney, G. J., M. E. Brazinski, B. E. Bouma, S. A. Boppart, C. Pitris, J. F. Southern and J. G. Fujimoto, In Vivo endoscopic optical biopsy with optical coherence tomography, Science 276, 2037 (1997).

Thompson, L. F., C. G. Willson, and M. J. Bowden, Introduction to Microlithography, 2nd edition, American Chemical Society, Washington, DC, 1994.

Wang, L., P. P. Ho, C. Liu, G. Zhang and R. R. Alfano, Ballistic 2-D imaging through scattering walls using an ultrafast Optical Kerr gate, Science 253, 769 (1991).

Wardlaw, N. C., J. Canadian Petrol. Tech. **21**, 21 (1982).